Onboard Real-Time Estimation of Vehicle Lateral Tire–Road Forces and Sideslip Angle

Moustapha Doumiati, Alessandro Correa Victorino, Ali Charara, *Member, IEEE*, and Daniel Lechner

***Abstract*—The principal concerns in driving safety with standard vehicles or cybercars are understanding and preventing risky situations. A close examination of accident data reveals that losing control of the vehicle is the main reason for most car accidents. To help to prevent such accidents, vehicle-control systems may be used, which require certain input data concerning vehicle-dynamic parameters and vehicle–road interaction. Unfortunately, some fundamental parameters, like tire–road forces and sideslip angle are difficult to measure in a car, for both technical and economic reasons. Therefore, this study presents a dynamic modeling and observation method to estimate these variables. One of the major contributions of this study, with respect to our previous work and to the largest literature in the field of the lateral dynamic estimation, is the fact that lateral tire force at each wheel is discussed in details. To address system nonlinearities and unmodeled dynamics, two observers derived from extended and unscented Kalman filtering techniques are proposed and compared. The estimation process method is based on the dynamic response of a vehicle instrumented with available and potentially integrable sensors. Performances are tested using an experimental car. Experimental results demonstrate the ability of this approach to provide accurate estimations, and show its practical potential as a low-cost solution for calculating lateral tire forces and sideslip angle.**

***Index Terms*—Lateral tire–road forces, sideslip angle, state observers, vehicle dynamics.**

I. Introduction

EXTENSIVE research has shown that over 90% of road accidents occur as a result of driver errors [1]: losing control of the vehicle, exceeding speed limits, leaving the road at high speed, etc. Preventing such accidents requires knowledge about the vehicle's motion. Since most drivers have a little knowledge of vehicle dynamics, driver assistance systems should be integrated.

Vehicle-control algorithms such as electronic stability control (ESC) systems have made great strides toward improving the handling and safety of vehicles. For example, experts estimate that ESC prevents 27% of loss-of-control accidents by intervening when emergency situations are detected [2]. While, nowadays, vehicle-control algorithms are undoubtedly a life-saving technology, they are limited by the available vehicle-state information.

Vehicle-control systems currently available on production cars rely on available inexpensive measurements, such as longitudinal velocity, accelerations, and yaw rate. Sideslip rate can be evaluated using yaw rate, lateral acceleration, and vehicle velocity [3]. However, calculating sideslip angle from sideslip rate integration is prone to uncertainty and errors from sensor bias. Besides, these control systems use unsophisticated, inaccurate tire models to evaluate lateral tire dynamics. In fact, measuring tire forces and sideslip angle is very difficult for technical, physical, and economic reasons. Therefore, these important data must be observed or estimated. If control systems were in possession of the complete set of lateral tire characteristics, namely lateral forces, sideslip angle, and the tire–road friction coefficient, they could greatly enhance vehicle handling and increase passenger safety.

As the motion of a vehicle is governed by the forces generated between the tires and the road, knowledge of the tire forces is crucial when predicting vehicle motion. For example, a vehicle can turn because of the applied lateral tire forces. In fact, what happens is that when the front wheels of a vehicle are steered, a slip angle is created, which gives rise to a lateral force. This lateral force turns or yaws the vehicle. Under normal driving situations (low slip angle), a vehicle responds predictably to the driver's inputs. As the vehicle approaches the handling limits, for example, during an evasive emergency maneuver, or when a vehicle undergoes high accelerations, high slip angle occurs and the vehicle's dynamic becomes highly nonlinear and its response becomes less predictable and potentially very dangerous.

Accurate data about tire forces and sideslip angle leads to a better evaluation of the road friction and the vehicle's possible trajectories, and to a better vehicle control. Moreover, it makes possible the development of a diagnostic tool for evaluating the potential risks of accidents related to poor adherence or dangerous maneuvers.

Lateral vehicle-dynamics estimation has been widely discussed in the literature. Several studies have been conducted regarding the estimation of tire–road forces and sideslip

Manuscript received March 1, 2009; revised May 30, 2009 and November 3, 2009; accepted March 6, 2010. Date of publication May 17, 2010; date of current version May 11, 2011. Recommended by Technical Editor Y. Li. This work was supported by the French National PREDIT-SARI-Research into Attributes for Advanced Diagnosis of Road Discontinuity project.

M. Doumiati is with the Institut National Polytechnique de Grenoble, Grenoble Cedex 38031, France, and also with the Heudiasyc Laboratory, Unités Mixtes de Recherche (UMR) Centre National de la Recherche Scientifique (CNRS) 6599, Centre de Recherche Royallieu, Université de Technologie de Compiègne, Compiégne BP20529-60205, France (e-mail: moustapha.doumiati@gmail.com).

A. C. Victorino and A. Charara are with the Heudiasyc Laboratory, Unités Mixtes de Recherche (UMR) Centre National de la Recherche Scientifique (CNRS) 6599, Centre de Recherche Royallieu, Université de Technologie de Compiègne, Compiègne BP20529-60205, France (e-mail: acorreav@hds.utc.fr; acharara@hds.utc.fr).

D. Lechner is with the Department of Accident Mechanism Analysis (Salon de Provence), French National Institute for Transport and Safety Research, Bron 13300, France (e-mail: daniel.lechner@inrets.fr).

Digital Object Identifier 10.1109/TMECH.2010.2048118

angle [4]–[9]. For example, Wenzel *et al.* [4] and Dakhlallah *et al.* [5], estimate the vehicle-dynamic states for a four-wheel vehicle model (FWVM) comprising 4 DOF. Consequently, tire forces are calculated based on the estimated states and using tire models. Ray [6] estimates the vehicle-dynamic states and lateral tire forces per axle for a 9 DOF vehicle model. Ray uses measures of the applied torques as inputs to his model. We note that the torque is difficult to get in practice; it requires expensive sensors. More recently, the authors of [7] and [8], proposed observers to estimate lateral forces per axle without using torque measures. Wilkin *et al.* [9] propose an estimation process based on a 3 DOF vehicle model, as a tire force estimator.

In [7]–[9], lateral forces are modeled with a derivative equal to random noise. Wilkin *et al.* [9] remark that such modeling leads to a noticeable inaccuracy when estimating individual lateral tire forces, but not in axle lateral forces. This phenomenon is due to the nonrepresentation of the lateral load transfer when modeling.

While the literature deals with lateral forces per axle, the main goal of this study is to develop an estimation method that uses a simple vehicle–road model and a certain number of valid measurements in order to estimate accuracy, and in real time, the lateral force at each individual tire–road contact point. We suppose a prior knowledge of road conditions. This study presents two particularities as follows.

1) The estimation process does not use the measurement of wheel torques.
2) As will be described in Section II, the estimation process uses accurate normal tire forces. Many approaches found in the literature assume constant vertical forces. However, during cornering, accelerating, and braking, the load distribution varies significantly in a car, which affects directly cornering stiffness and lateral forces evaluation.

The observation system is highly nonlinear and presents unmodeled dynamics. For these reasons, two observers based on the extended Kalman filter (EKF) and the unscented Kalman filter (UKF) are proposed. EKF is probably the most commonly used estimator for nonlinear systems. However, UKF has proved to be a superior alternative, especially when the system presents strong nonlinearities. This study compares and discusses these two filtering techniques in our estimation approach.

In order to show the effectiveness of the estimation method, some validation tests were carried out on an instrumented vehicle in realistic driving situations.

The remainder of the paper is organized as follows. Section II describes briefly the estimation-process algorithm. Section III presents the vehicle model. In Section IV, tire–road interaction is discussed. Section V describes the developed observers in this study, and presents the observability analysis. In Section VI, the observers are discussed and compared to real-experimental data. Finally, we make some concluding remarks regarding our study and future perspectives.

II. Estimation Process Description

The estimation process is shown in its entirety by the block diagram in Fig. 1, where a_x and a_{ym} are the longitudinal and lateral accelerations, respectively, $\dot{\psi}$ is the yaw rate, $\dot{\theta}$ is the roll rate, Δ_{ij} [i represents the front (1) or the rear (2) and j represents the left (1) or the right (2)] is the suspension deflection, w_{ij} is the wheel velocity, F_{zij} and F_{yij} are the normal and lateral tire–road forces, respectively, and β is the sideslip angle at the Center Of Gravity (COG). The estimation process consists of two blocks, and its role is to estimate sideslip angle at the COG, normal, and lateral forces at each tire/road contact point, and consequently, evaluate the used lateral friction coefficient. The following measurements are needed:

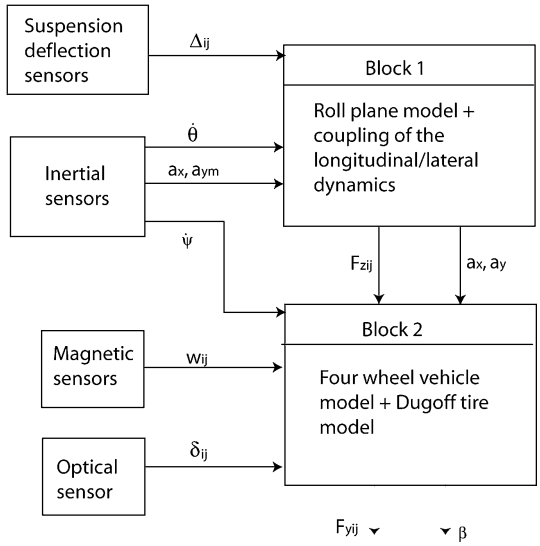

Fig. 1. Estimation process: block diagram.

1) yaw and roll rates measured by gyrometers;
2) longitudinal and lateral accelerations measured by accelerometers;
3) suspension deflections using suspension deflections sensors;
4) steering angle measured by an optical sensor;
5) rotational velocity for each wheel given by magnetic sensors.

The first block aims to provide the vehicle's mass, lateral load transfer, normal tire forces, and the corrected lateral acceleration a_y (by canceling the gravitational acceleration component that distorts the accelerometer signal a_{ym}). It contains observers based on vehicle's roll dynamics and model that couples longitudinal and lateral accelerations. We have looked at the first block in previous studies [10], [11]. This paper focuses only on the second block, whose main role is to estimate individual lateral tire force and sideslip angle. The second block makes use of the estimations provided by the first block. In fact, as will be shown in Section IV-A, the impact of including accurate normal forces in the calculation of lateral forces is fundamental.

One specificity of this estimation process is the use of blocks in series. By using cascaded observers, the observability problems entailed by an inappropriate use of the complete modeling equations are avoided, enabling the estimation process to be carried out in a simple and practical way.

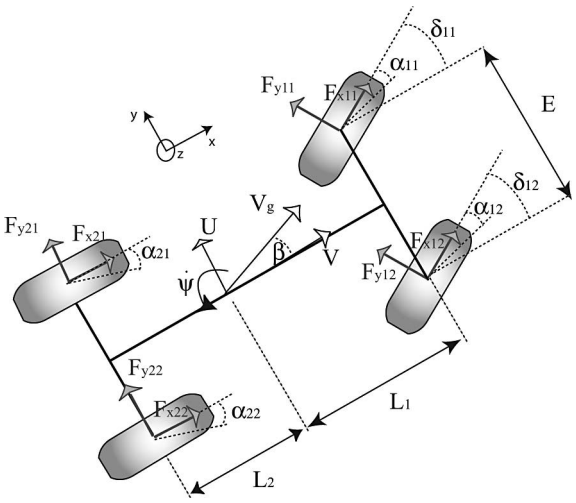

Fig. 2. Four-wheel vehicle model.

III. Four-Wheel Vehicle Model

The FWVM is chosen for this study because it is simple and corresponds sufficiently to our objectives. The FWVM is widely used to describe transversal vehicle-dynamic behavior [5], [6], [8], [12].

Fig. 2 shows a simple diagram of the FWVM model in the longitudinal and lateral planes. In order to simplify the lateral and longitudinal dynamics, rolling resistance is neglected. Additionally, the front and rear track widths (E) are assumed to be equal. L_1 and L_2 represent the distance from the vehicle's COG to the front and rear axles, respectively. The sideslip at the vehicle COG (β) is the difference between the velocity heading (V_g) and the true heading of the vehicle (ψ). The yaw rate ($\dot{\psi}$) is the angular velocity of the vehicle about the COG. The forward and lateral velocities are V and U, respectively. The longitudinal and lateral forces ($F_{x,y,i,j}$) are shown for front and rear tires of the vehicle.

Longitudinal forces should be taken into account to enable accurate lateral forces estimation during vehicle braking or acceleration. While considering their effect is certainly important, its inclusion makes solving the lateral estimation problem considerably more complex. Thus, it may be desirable to solve the lateral estimation problem in the absence of longitudinal forces first and include them in later studies. This can be done by focusing on solving the estimation problem when the vehicle is driven at constant speeds [13]. This study extended the hypothesis of moving in a constant speed and addresses the case of a front-wheel drive, where rear longitudinal forces are neglected relative to the front longitudinal forces. Longitudinal front axle forces are considered by assuming that

$$F_{x1} = F_{x11} + F_{x12}. \tag{1}$$

The longitudinal force evolution is modeled with a random walk model, where its derivative is equal to random noise ($\dot{F}_{x1} = 0$). This is due to the lack of knowledge on the longitudinal slip and the effective radius of the tires.

The lateral dynamics of the vehicle can be obtained by summing the forces and moments about the vehicle's COG. Consequently, the simplified FWVM is formulated as the following dynamic relationships:

$$\begin{cases} \dot{V}_g = \dfrac{1}{m}\begin{bmatrix} F_{x1}\cos(\beta-\delta) + F_{y11}\sin(\beta-\delta) \\ +F_{y12}\sin(\beta-\delta) + (F_{y21}+F_{y22})\sin\beta \end{bmatrix} \\ \ddot{\psi} = \dfrac{1}{I_z}\begin{bmatrix} L_1[F_{y11}\cos\delta + F_{y12}\cos\delta + F_{x1}\sin\delta] \\ -L_2[F_{y21}+F_{y22}] \\ +\dfrac{E}{2}[F_{y11}\sin\delta - F_{y12}\sin\delta] \end{bmatrix} \\ \dot{\beta} = \dfrac{1}{mV_g}\begin{bmatrix} -F_{x1}\sin(\beta-\delta) + F_{y11}\cos(\beta-\delta) \\ +F_{y12}\cos(\beta-\delta) + (F_{y21}+F_{y22})\cos\beta \end{bmatrix} - \dot{\psi} \\ a_y = \dfrac{1}{m}[F_{y11}\cos\delta + F_{y12}\cos\delta + (F_{y21}+F_{y22}) + F_{x1}\sin\delta] \\ a_x = \dfrac{1}{m}[-F_{y11}\sin\delta - F_{y12}\sin\delta + F_{x1}\cos\delta] \end{cases} \tag{2}$$

where m is the vehicle mass and I_z is the yaw moment of inertia.

The tire slip angle (α_{ij}), as shown in Fig. 2, is the difference between the tire's longitudinal axis and the tire's velocity vector. The tire velocity vector can be obtained from the vehicle's velocity (at the COG) and the yaw rate. Assuming that rear steering angles are approximately null, the direction or heading of the rear tires is the same as that of the vehicle. The heading of the front tires includes the steering angle (δ). The front steering angles are assumed to be equal ($\delta_{11} = \delta_{12} = \delta$). The forward velocity V, steering angle δ, yaw rate $\dot{\psi}$, and the vehicle body slip angle β are then used to calculate the tire slip angles α_{ij}, where

$$\begin{cases} \alpha_{11} = \delta - \arctan\left[\frac{V\beta + L_1\dot{\psi}}{V - E\dot{\psi}/2}\right] \\ \alpha_{12} = \delta - \arctan\left[\frac{V\beta + L_1\dot{\psi}}{V + E\dot{\psi}/2}\right] \\ \alpha_{21} = -\arctan\left[\frac{V\beta - L_2\dot{\psi}}{V - E\dot{\psi}/2}\right] \\ \alpha_{22} = -\arctan\left[\frac{V\beta - L_2\dot{\psi}}{V + E\dot{\psi}/2}\right]. \end{cases} \tag{3}$$

Assuming small tire slip angles, the wheel–ground contact point velocities Vw_{ij} depend on the vehicle COG velocity V_g according to the following relations:

$$\begin{cases} Vw_{11} = V_g - \dot{\psi}(E/2 - L_1\beta) \\ Vw_{12} = V_g + \dot{\psi}(E/2 + L_1\beta) \\ Vw_{21} = V_g - \dot{\psi}(E/2 + L_2\beta) \\ Vw_{22} = V_g + \dot{\psi}(E/2 - L_2\beta). \end{cases} \tag{4}$$

IV. Tire–Road Interaction

As the motion of a vehicle is governed by the forces generated between the tires and the road, knowledge of the tire forces is crucial in order to predict the vehicle's motion. This section presents the tire–road interaction phenomenon, especially the lateral tire forces. Since the quality of the observer largely depends on the accuracy of the tire model, the underlying model

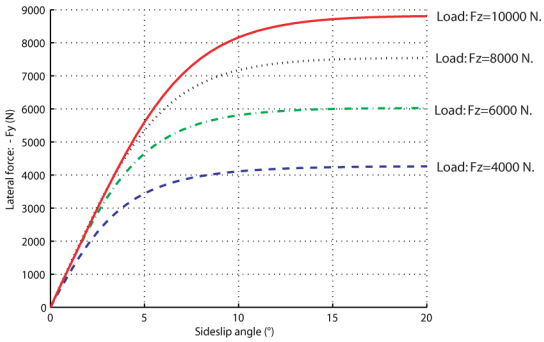

Fig. 3. Generic tire curve: lateral force versus slip angle.

must be precise. Taking real-time calculation requirement, the tire model should also be simple.

A. Lateral Tire–Force Model

The pneumatic tires on a vehicle can create both lateral and longitudinal forces, allowing the car to accelerate, brake, and turn. These forces are a function of the tire properties (including material, tread pattern, and pressure), the normal load on the tire, and the velocities experienced by the tire. The relation between these factors is extremely complex and nonlinear. Several models that predict well the behavior of tires have been developed. Many different tire models, based on the physical nature of the tire and/or on empirical formulations deriving from experimental data, can be found in the literature. These models include the Burckhardt, Dugoff, and Pacejka models [12], [14], [15]. One of the most commonly used model is the Pacejka's "magic formula." It does an excellent job of predicting real-tire behavior. However, it requires a large number of tire-specific parameters that are usually unknown. Another commonly used model is the Dugoff tire model. It synthesizes all the tire property parameters into two constants Cx and Cy, referred to as the longitudinal and cornering stiffness of the tire. Dugoff's model is the one used in this study. Neglecting longitudinal forces, the simplified nonlinear lateral tire forces are given by

$$F_{yij} = -Cy_{ij}\tan\alpha_{ij} f(\lambda) \tag{5}$$

where Cy_{ij} is the lateral stiffness, α_{ij} is the slip angle, and $f(\lambda)$ is given by

$$f(\lambda) = \begin{cases} (2-\lambda)\lambda, & \text{if} \quad \lambda < 1 \\ 1, & \text{if} \quad \lambda \geq 1 \end{cases} \tag{6}$$

$$\lambda = \frac{\mu F_{zij}}{2Cy_{ij}\,|\tan\alpha_{ij}|}. \tag{7}$$

In the aforementioned formulation, μ is the lateral friction coefficient and F_{zij} is the normal load on the tire. This simplified tire model assumes pure slip conditions with negligible longitudinal slip, a uniform pressure distribution, a rigid tire carcass, and a constant friction coefficient for sliding rubber. As shown in (5), vertical forces and the tire slip angles can be used to find the lateral force on each tire. Fig. 3 is a graph of the lateral force versus tire slip angle. It will be noted that as the load increases, the peak lateral force occurs at somewhat higher slip angle.

It is clear that for small slip angles, the force profile can be defined by a linear region. When operating in this region, a vehicle responds predictably to the driver's inputs.

As the slip angle continues to grow, the tire begins to saturate and reach a peak value; this area is commonly called the nonlinear region of the tire curve. It represents the tire limits and it is rarely reached under normal driving conditions. If the front tires saturate first, the vehicle is said to display limit understeer, and may plow out of a bend. If the rear tires saturate first, the vehicle limit oversteers and may spin out. Because most drivers are not accustomed to operate in the nonlinear handling regime, both of these responses are potentially very dangerous.

B. Further Consideration for Cornering Stiffness

The original Dugoff tire model has a constant stiffness in respect to weight transfer. However, according to [16], load transfer affects the cornering stiffness. It can be represented by a second-order polynomial with respect to the normal force, as shown as follows:

$$Cy_{ij}(F_z) = (aF_{zij} - bF_{zij^2}) \tag{8}$$

where a and b are the first- and second-order coefficient in the cornering stiffness polynomial, respectively.

This study proposes a modified Dugoff tire model, where the cornering stiffness varies with respect to load.

C. Dynamic Tire Model

When vehicle sideslip angle changes, a lateral tire force is created with a time lag. This transient behavior of tires can be formulated using a relaxation length σ. The relaxation length is the distance covered by the tire while the tire force is kicking in. Using the relaxation model presented in [17] with the assumption of small slip angle, the dynamic lateral forces can be written as follows:

$$\dot{F}_{yij} = \frac{V_g}{\sigma_i}(-F_{yij} + \overline{F_{yij}}) \tag{9}$$

where $\overline{F}_{yij}$ is calculated from the quasi-static Dugoff tire–force model and σ_i is the relaxation length. For further information concerning tire transient behavior, refer to [18].

V. Observers Design

This section presents a description of the observer devoted to lateral tire forces and sideslip angle. The state-space formulation, the observability analysis, and the estimation method will be presented.

A. Stochastic State-Space Representation

The nonlinear stochastic state-space representation of the system described in previous section is given as follows:

$$\begin{cases} \dot{X}(t) = f(X(t), U(t)) + w(t) \\ Y(t) = h(X(t), U(t)) + v(t). \end{cases} \tag{10}$$

The input vector U comprises the steering angle and the normal forces considered estimated by the first block (see Fig. 1)

$$U = [\delta, F_{z11}, F_{z12}, F_{z21}, F_{z22}]^T = [u_1, u_2, u_3, u_4, u_5]^T. \tag{11}$$

The measure vector Y comprises yaw rate, vehicle velocity (approximated by the mean of the rear wheel velocities calculated from wheel-encoder data), longitudinal, and lateral accelerations

$$Y = [\dot{\psi}, V_g, a_x, a_y]^T = [y_1, y_2, y_3, y_4]^T. \tag{12}$$

The state vector X comprises yaw rate, vehicle velocity, sideslip angle at the COG, lateral forces, and the sum of the front longitudinal tire forces

$$\begin{aligned} X &= [\dot{\psi}, V_g, \beta, F_{y11}, F_{y12}, F_{y21}, F_{y22}, F_{x1}]^T \\ &= [x_1, x_2, x_3, x_4, x_5, x_6, x_7, x_8]^T. \end{aligned} \tag{13}$$

The process and measurements noise vectors w and v, respectively, are assumed to be white, zero mean, and uncorrelated.

Consequently, the particular nonlinear function $f(.)$ of the state equations is given by

$$\begin{cases} f_1 = \dfrac{1}{I_z}\begin{bmatrix} L_1[x_4\cos u_1 + x_5\cos u_1 + x_8\sin u_1] \\ -L_2[x_6 + x_7] \\ +\dfrac{E}{2}[x_4\sin u_1 - x_5\sin u_1] \end{bmatrix} \\ f_2 = \dfrac{1}{m}\begin{bmatrix} x_8\cos(x_3 - u_1) + x_4\sin(x_3 - u_1) \\ +x_5\sin(x_3 - u_1) + (x_6 + x_7)\sin(x_3) \end{bmatrix} \\ f_3 = \dfrac{1}{mx_2}\begin{bmatrix} -x_8\sin(x_3 - u_1) + x_4\cos(x_3 - u_1) \\ +x_5\cos(x_3 - u_1) + (x_6 + x_7)\cos x_3 \end{bmatrix} - x_1 \\ f_4 = \dfrac{x_2}{\sigma_1}(-x_4 + \overline{F_{y11}}(\alpha_{11}, u_2)) \\ f_5 = \dfrac{x_2}{\sigma_1}(-x_5 + \overline{F_{y12}}(\alpha_{12}, u_3)) \\ f_6 = \dfrac{x_2}{\sigma_2}(-x_6 + \overline{F_{y21}}(\alpha_{21}, u_4)) \\ f_7 = \dfrac{x_2}{\sigma_2}(-x_7 + \overline{F_{y22}}(\alpha_{22}, u_5)) \\ f_8 = 0. \end{cases} \tag{14}$$

The observation function $h(.)$ is as follows:

$$\begin{cases} h_1 = x_1 \\ h_2 = x_2 \\ h_3 = \dfrac{1}{m}[-x_4\sin u_1 - x_5\sin u_1 + x_8\cos u_1] \\ h_4 = \dfrac{1}{m}[x_4\cos u_1 + x_5\cos u_1 + (x_6 + x_7) + x_6\sin u_1]. \end{cases} \tag{15}$$

The state vector $X(t)$ will be estimated by applying the EKF and UKF techniques: observers O_{EKF} and O_{UKF}, respectively, (see Section V-C).

B. Observability

Observability is a measure of how well the internal states of a system can be inferred from knowledge of its inputs and external outputs. This property is often presented as a rank condition on the observability matrix. Using the nonlinear state-space formulation of the system presented in Section V-A, the observability definition is local and uses the Lie derivative [19].

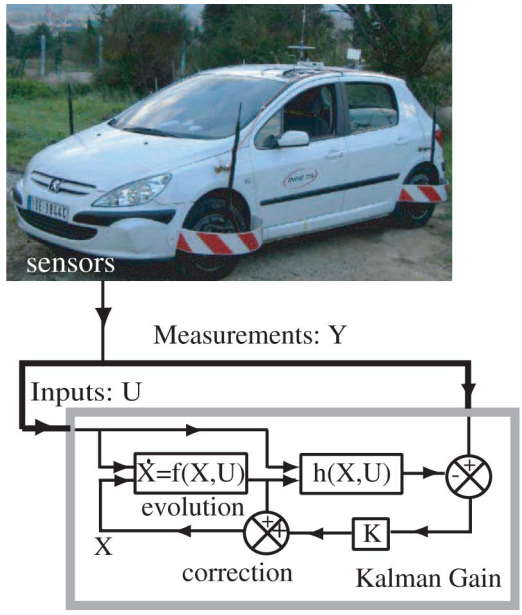

Fig. 4. Estimation process (continuous time).

An observability analysis of this system was undertaken in [20]. It was shown that the system is observable except when:

1) steering angles are null;
2) the vehicle is at rest ($V_g = 0$).

For these situations, we assume that lateral forces and sideslip angle are null, which approximately corresponds to the real cases.

C. Estimation Method: Extended Versus Unscented Filtering Techniques

The aim of an observer or a virtual sensor is to estimate a particular unmeasurable variable from available measurements and a system model in a closed-loop observation scheme, as illustrated in Fig. 4. A simple example of an open-loop observer is the model given by relation (1). Because of the system-model mismatch (unmodeled dynamics, parameter variations, etc.) and the presence of unknown and unmeasurable disturbances, the calculation obtained from the open-loop observer would deviate from the actual values over time. In order to reduce the estimation error, at least some of the measured outputs are compared to the same variables estimated by the observer. The difference is fed back into the observer after being multiplied by a gain matrix K, and therefore, we have a closed-loop observer (see Fig. 4).

The observer was implemented in a first-order Euler approximation discrete form. At each iteration, the state vector is first calculated according to the evolution equation, and then, corrected online with the measurement errors (innovation) and filter gain K in a recursive prediction-correction mechanism.

The gain K calculation for nonlinear system is quite a challenge. Therefore, many approaches are developed in order to set K. We may find the sliding mode (SM), the extended

Luenberger (EL), and the Kalman estimation methods. The SM is a well-known estimation method characterized by its robustness against systems parameter variations [21]. However, we believe that using this method, it could be hard to calculate K by introducing complicated Lyapunov functions, especially that our model is represented by many states. Moreover, the SM can suffer also from the "chattering" problem [22]. The EL is usually introduced for deterministic systems [23]. However, taking into account the different unmodeled dynamics and the parameter variations of our model, we believe that a stochastic filter can be more efficient than an EL. The Kalman filter presents the advantages to be a stochastic filter simply formulated. It is an optimal recursive data-processing algorithm and is widely represented in [24] and [25] (note that optimality is conserved under some constraints). These assumptions lead us to calculate K by selecting the Kalman filter tools. The Kalman filter is widely used in the automotive field [26], [27]. In the Appendix, a brief description of the EKF and UKF algorithms is presented.

First, the observer O_{EKF} is developed in order to estimate the state vector $X(t)$ (see Section V-A). Certain difficulties have to be addressed, in particular:

1) the high nonlinearities of the model, especially when the tires enter a nonlinear zone;
2) the calculation complexity of the Jacobian matrices, which causes implementation difficulties.

To overcome all of these restrictions, the observer O_{UKF} is proposed. UKF is introduced to improve EKF, especially for strongly nonlinear systems. For these systems, the first-order linearization of the EKF algorithm using Jacobian matrices is not sufficient, and linearization errors are significant. UKF acts directly on the nonlinear model and approximates the states by using a set of sigma points, thus avoiding the linearization associated with EKF [28], [29]. UKF is a powerful nonlinear estimation technique that has proved a superior alternative to EKF in many robotics applications.

D. Filter Settings

We remember that the computation of the EKF gain is a subtle mix between process and observation noises, Q and R, respectively. The less noise in the operation compared to the uncertainty in the model, the more the variables will be adapted to follow measurements.

Since the lateral forces are modeled using a relaxation model based on reliable tire models, the uncertainty we put on them is not too high. However, the longitudinal force per front axle is not modeled at all, hence, it is represented by a high noise level. The other states (yaw rate, longitudinal, and lateral vehicle velocity) are modeled using the vehicle's equations. Therefore, they are said to have an average noise. However, since the embedded sensors have good accuracy, the noises on the measurements are quite small. In order to reduce the complexity of the problem, both measurement covariance matrix and the process covariance matrix are assumed to be constant and diagonal. The off-diagonal elements are set to 0. This means that both the measurement noises and the process noises are supposed uncorrelated.

Fig. 5. Experimental vehicle.

In addition to R and Q, the UKF has other parameters to tune. These parameters, named α, β_t, and ϵ determine the scaling parameter of the unscented transformation (see Appendix) [28], [29]. The parameter α determines the spread of the sigma points around the estimation, and is usually set $10^{-4} \leq \alpha \leq 1$. In our application, we choose α equal 0.5. The constant β_t is used to incorporate part of the prior knowledge of the distribution of X, and for Gaussian distributions $\beta_t = 2$ is optimal. The parameter ϵ is set to 0.

VI. Experimental Results

In this section, we present the experimental car used to test the observers potential, and we discuss and analyze the test conditions and the observers' results.

A. Experimental Car

The experimental vehicle shown in Fig. 5 is the INRETS-MA (Département Mécanismes d'Accidents, Institut National de la Recherche sur les Transports et leur Sécurité) Laboratory's test vehicle [3]. It is a Peugeot 307 equipped with:

1) gyrometers and accelerometers that measure the rotations (roll, pich and yaw rates) and accelerations (longitudinal, lateral and vertical) of the car body, respectively;
2) suspension sensors that measure the distances between the wheels and the car body;
3) three correvit noncontact optical sensors:
    a) one correvit is located in chassis rear overhanging position and it measures longitudinal and lateral vehicle speeds;

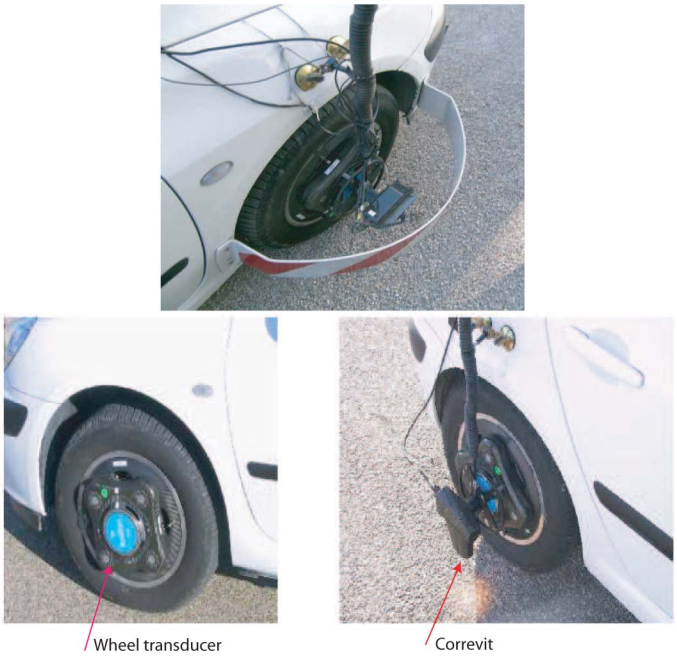

Fig. 6. Wheel-force transducer and sideslip sensor installed at the tire level.

b) two correvits are installed on the front right and rear right tires, and they measure front and rear tires velocities and sideslip angles;

4) dynamometric wheels fitted on all four tires, which are able to measure tire forces and wheel torques in and around all three dimensions;
5) steering angle sensors;
6) magnetic sensors that measure rotational velocity for each wheel.

It is important to note that the correvit and the wheel-force transducer (see Fig. 6) are very expensive sensors. They are used in this study as a reference for validating the estimation process.

The car is fitted with an acquisition device based on an industrial PC including 64 analog channel boards and a proprietary acquisition software developed in C/C++. The signals of the sensors are sampled at 100 Hz, and processed by antialiasing filters. The PC is located in the back of the car with all the electronics, the operator is on the front right seat with a monitor, keyboard, and several switches to manage the acquisition. Consequently, data is recorded in a file.

The acquisition device was developed to include the observers as external functions. Observers are written in C/C++ and are embedded as a real-time applications under dynamic-link library (DLL) form. The DLLs call the data they need from the acquisition, compute, and estimate the required information and send them back to the acquisition software, to be included in the results file.

B. Test Conditions

Test data from nominal as well as adverse driving conditions were used to assess the performance of the observer presented in Section V, in realistic driving situations. We report a

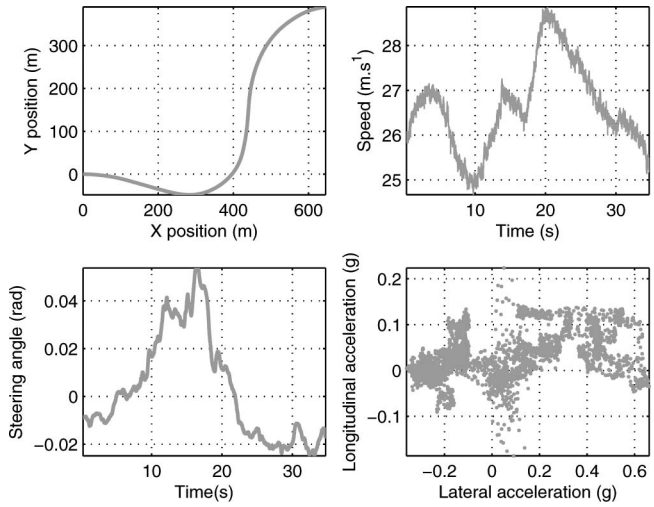

Fig. 7. Experimental test: vehicle trajectory, speed, steering angle, and acceleration diagrams for the lane-change test.

"right–left–right bend combination" maneuver (one of a number of experimental tests that we carried out), where the dynamic contributions play an important role. Fig. 7 presents the Peugeot's trajectory, its speed, steering angle, and "g–g" acceleration diagram during the course of the test. The acceleration diagram, that determines the maneuvering area utilized by the driver/vehicle, shows that large lateral accelerations were obtained (absolute value up to $0.6g$). This means that the experimental vehicle was put in a critical driving situation.

This experimental test is done on a dry road surface that shows normally a high μ value. In this study, longitudinal slips are ignored, and the road friction is assumed equal to the lateral road friction.

Although the friction coefficient is not only dependent on road conditions, but also on tire conditions (inflation pressure, temperature, etc.), researches try to classify the road in categories, like dry asphalt, wet asphalt, etc. According to [30], the average μ value for a dry surface is between 0.9 and 1.1. Therefore, for this test, μ is assumed set to 0.9 when using (7).

C. Validation of Observers

The observer results are presented in two forms: as tables of normalized errors and as figures comparing the measurements and the estimations. The normalized error for an estimation z is defined as follows:

$$\epsilon_z = 100 \times \frac{\|z_{\text{obs}} - z_{\text{measured}}\|}{\max(\|z_{\text{measured}}\|)} \tag{16}$$

where z_{obs} is the variable calculated by the observer, z_{measured} is the measured variable, and $\max(\|z_{\text{measured}}\|)$ is the absolute maximum value of the measured variable during the test maneuver.

Figs. 8–11 show lateral forces on the front and rear wheels. According to these plots, the observers are relatively good with respect to measurements. Some small differences during the trajectory are to be noted. These might be explained by neglected geometrical parameters, especially the camber angles, which

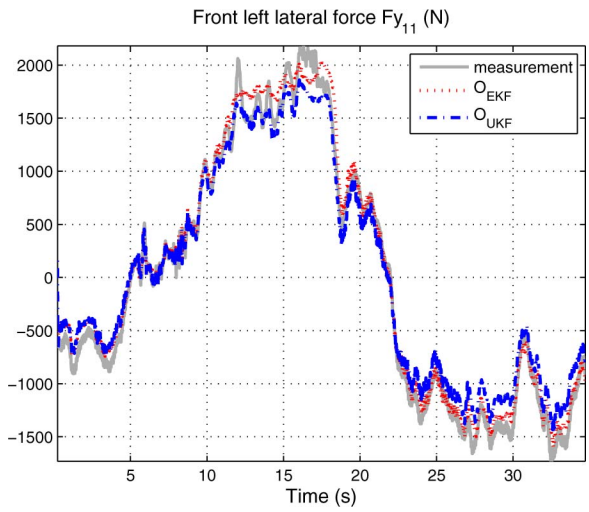

Fig. 8. Estimation of front left-hand lateral tire force.

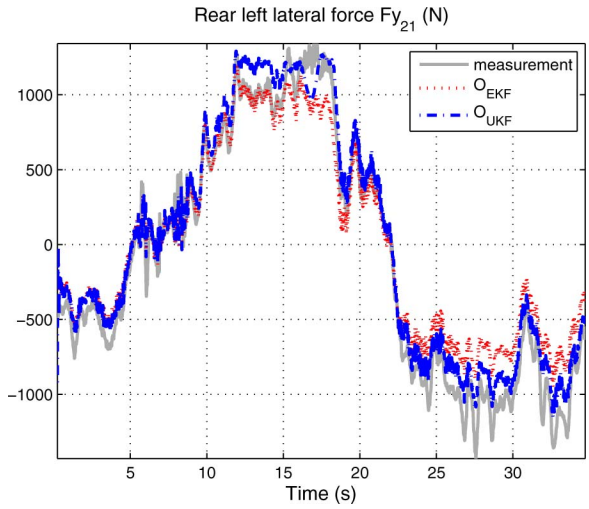

Fig. 9. Estimation of rear left-hand lateral tire force.

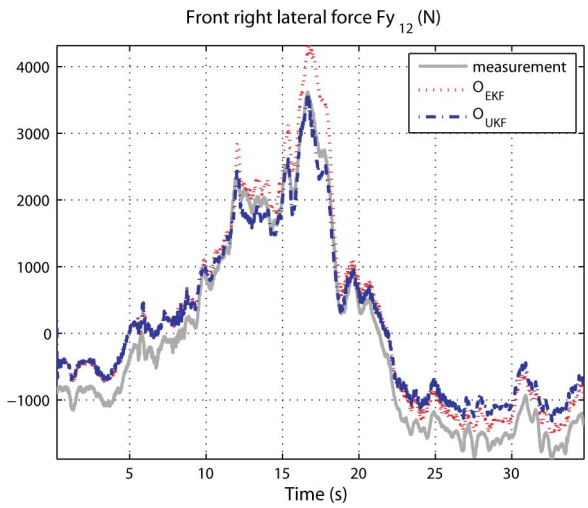

Fig. 10. Estimation of front right-hand lateral tire force.

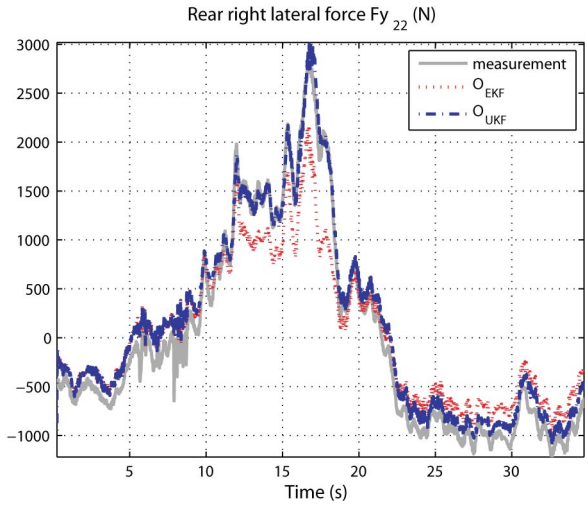

Fig. 11. Estimation of rear right-hand lateral tire force.

also produce a lateral forces component [31]. It is also shown that the lateral forces on the right-hand tires exceed those on the left-hand tires. This result is clearly a consequence of the load transfer produced during cornering from the left to the right-hand side of the vehicle. In fact, as explained in Section IV-A, lateral force increases as normal force increases. Figs. 12 and 13, deduced from the first block of the whole estimation process, show the variations of the normal forces on the right and left tires.

Fig. 14 represents the front longitudinal tire force. This reported result is good and it shows the observer's ability to reconstruct the longitudinal forces per front axle, even by considering a simple random walk model. Although the vehicle accelerates and brakes during the maneuvre, the obtained results are accurate. It is important to note the observer's robustness with respect to velocity variations.

Fig. 15 represents the vehicle's velocity at the COG over the entire trajectory. The vehicle velocity at the COG was calculated

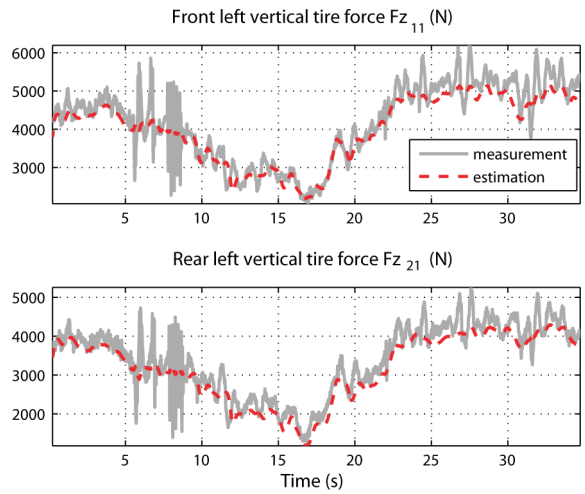

Fig. 12. Variations of the normal forces on the left tires.

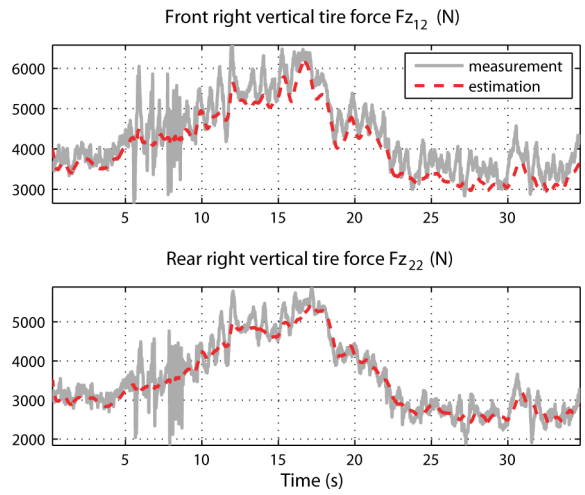

Fig. 13. Variations of the normal forces on the right tires.

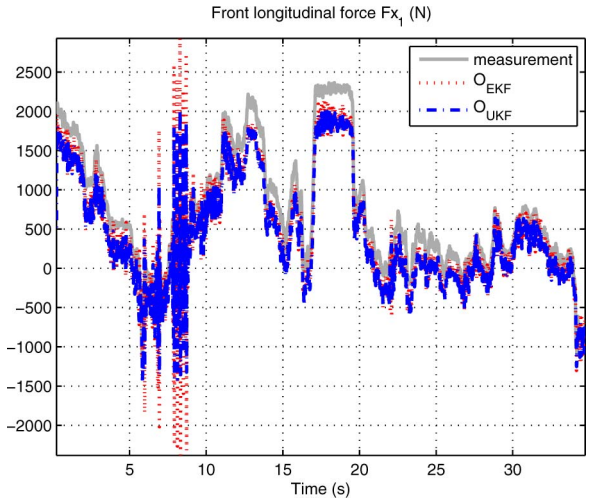

Fig. 14. Estimation of front longitudinal tire force.

as a function of Vw_{22}, according to (3), where Vw_{22} is measured by the correvit sensor.

Having estimated the vehicle sideslip angle at the COG, it is possible to calculate the tires slip angle from (2). Figs. 16 and 17 show how sideslip angle changes during the test. Reported results are relatively good.

Table I presents maximum absolute values, normalized mean errors, and normalized standard deviations (std) for vehicle velocities, lateral tire forces, and sideslip angles. Despite the simplicity of the model, we can deduce that for this test, the performance of the observers, notably O_{UKF}, is satisfactory, with normalized error globally less than 9%.

D. Comparison Between O_{EKF} and O_{UKF}

If we compare the two observers, we can confirm that O_{UKF} is more efficient. In fact, during the time interval (12–18 s), when heavy demands are made on the vehicle, the observer O_{EKF} does not converge well. This phenomenon is due to the intense nonlinearities of the vehicle dynamics and tires behavior. This means that the first-order linearization of the EKF algorithm

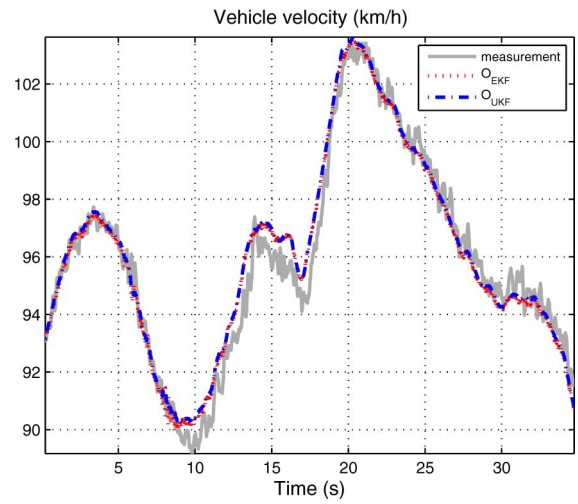

Fig. 15. Estimation of vehicle velocity.

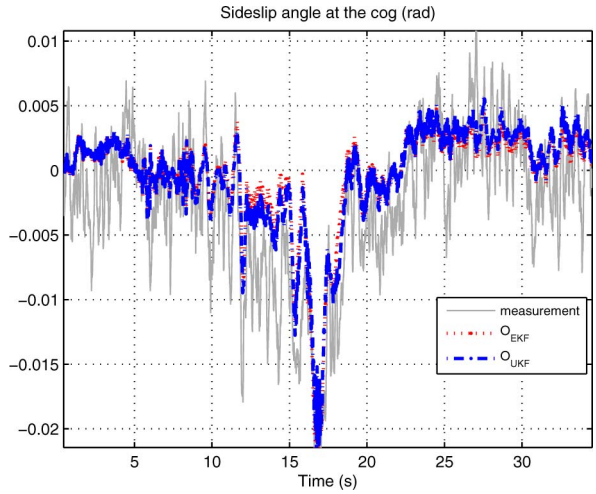

Fig. 16. Estimation of the sideslip angle at the COG.

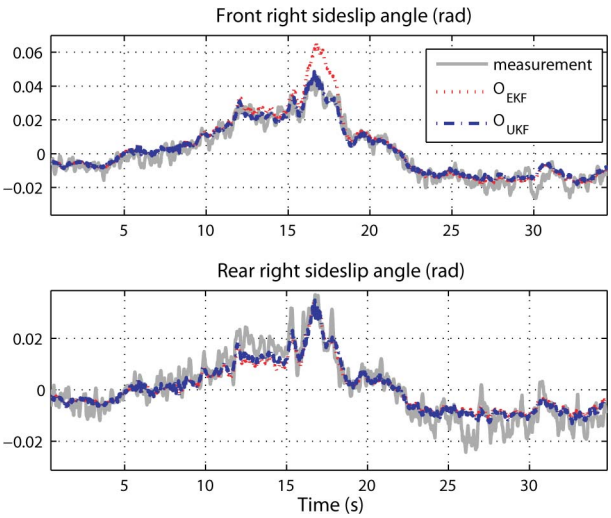

Fig. 17. Estimation of the tire slip angles.

TABLE I
OBSERVERS O_{EKF} AND O_{UKF}: MAXIMUM ABSOLUTE VALUES, NORMALIZED MEAN ERRORS, AND NORMALIZED STD

EKF \ UKF	Max |||	Mean %	Std %
Fy_{11}	2180 (N)	4.87 / 5.02	3.75 / 3.51
Fy_{12}	3617 (N)	9.7 / 9.32	4.07 / 4.30
Fy_{21}	1342 (N)	11.98 / 7.55	9.14 / 5.33
Fy_{22}	2817 (N)	10.12 / 5.07	6.96 / 2.92
Fx_1	2365 (N)	12.12 / 9.61	11.81 / 7.32
V_g	103.42 (km/h)	0.51 / 0.47	0.42 / 0.38
β	0.023 (rad)	13.4 / 10.20	10.42 / 9.52
α_{12}	0.026 (rad)	8.74 / 7.44	9.57 / 7.85
α_{22}	0.0243 (rad)	9.22 / 8.34	9.45 / 7.65

is no longer sufficient, and that the linearization errors become high. The UKF algorithm shows its ability to overcome this difficulty.

To get a full picture of the experimental test performance and the observer's behavior, we have to analyze the accelerations diagram and to look also at the lateral load transfer that happens during maneuvre. From Figs. 12 and 13, we can deduce that a huge lateral load transfer of about 6000 N is produced during the test. This means that the vehicle is highly solicited, and therefore, many unmodeled mechanical phenomenons intervene, especially the camber angles and the suspension kinematics that also cause tracks width variations. Furthermore, as a result of high lateral accelerations, we believe that the vehicle's COG position changes significantly, which also induces L_1 and L_2 variations. Regarding all these model mismatches, the O_{UKF} shows a robustness superiority with respect to O_{EKF}.

Another fundamental advantage offered by the UKF is avoiding the derivation of the Jacobian matrices that are nontrivial, especially when including the reference tire model, which itself depends on other states. This concept leads to implementation simplifications. Consequently, the observer O_{UKF} can be considered as the more appropriate estimator in our application.

E. Identification and Analysis of the Used Lateral Friction Coefficient

Knowing the road friction is essential for improving road safety. In fact, the maximum lateral friction coefficient of a given road indicates the maximum available lateral force, which, in turn, defines the vehicle's handling limit. In the literature, we can find some studies that deal with the maximum friction coefficient estimation [32], [33]. This study shows relevant results concerning the used lateral friction.

Given the vertical and lateral tire forces at each tire–road contact level, the estimation process is able to evaluate the used or mobilized lateral friction coefficient ρ. This is defined as the ratio of friction force to normal force, and is given by [31]

$$\rho_{ij} = \frac{F_{yij}}{F_{zij}}. \tag{17}$$

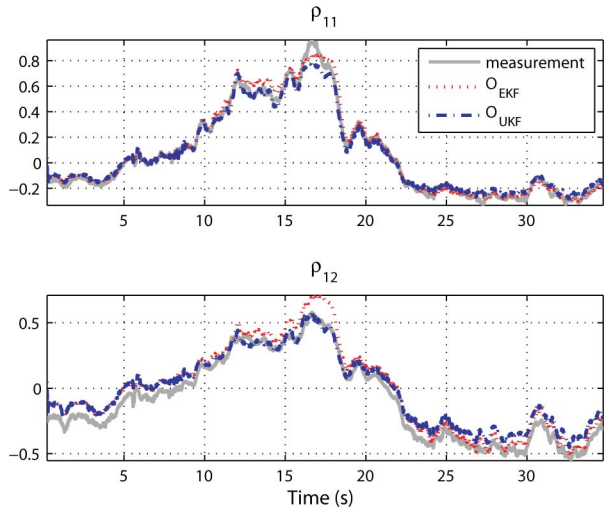

Fig. 18. Used lateral friction coefficients developed by the front tires.

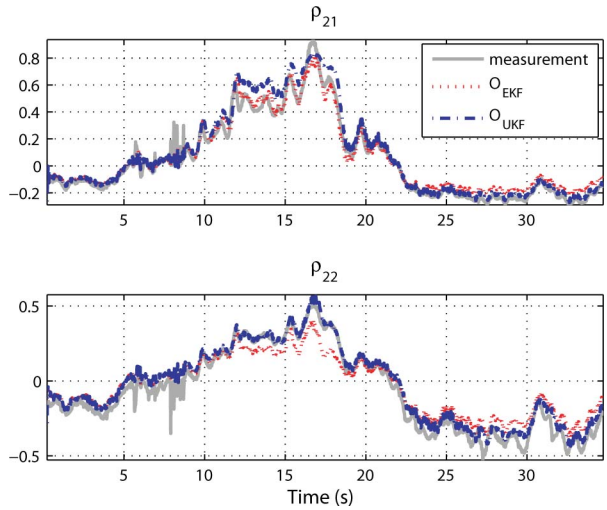

Fig. 19. Used lateral friction coefficient developed by the rear tires.

The lateral friction coefficients in Figs. 18 and 19 show that the estimated ρ_{ij} are close to the measured values. A closer investigation reveals that the used lateral friction coefficients ρ_{12} and ρ_{22} corresponding to the overloaded tires during cornering are lower than ρ_{11} and ρ_{21}. This phenomenon is due to the tire load sensitivity effect: the lateral friction coefficient is normally higher for the lighter loads, or conversely, diminishes as the load increases [31].

This test also demonstrates that ρ_{11} and ρ_{21} are high, especially for lateral accelerations up to 0.6, and that they attain the limit for the dry road friction coefficient. In fact, dry road surfaces show a high friction coefficient in the range 0.9–1.2 (implying that driving on these surfaces is safe), which means that for this test the limits of handling were reached.

The friction coefficient evaluation is important for evaluating the ratio of the used friction and for determining the available remainder.

F. Observers Robustness

1) Robustness With Respect to Road Variation: The tire–road friction coefficient μ depends on the tire characteristics and the road states. Therefore, a precise determination of this parameter is one of the biggest problems in vehicle-dynamics research. In this study, we have supposed a prior knowledge of the approximate value of μ. In the following, let us test the observers performance with respect to μ variations.

In the frame work of the National French PREDIT/ SARI/RADARR, the developed observers in this study were tested in a multitude of situations, especially on different dry roads with different characteristics. The results were always satisfactory.

At what limits could these observers be robust with respect to road variations? Are they able to function on a dry asphalt or a dry concrete road with the same performance? Are they able to work well in an iced road? To answer these questions, we propose to reconsider the "right–left–right bend combination" a test done on a dry road ($\mu = 0.9$), while this time, the parameter μ is supposed varying between -15% and $+15\%$ around its previously used value. Fig. 20 represents the normalized mean errors calculated according to (16). For simplicity reasons, we only illustrate the data corresponding to the rear tires. Each bar in Fig. 20 corresponds to a step variation of 5%. From the obtained results, we can deduce the following.

a) Globally, the observers performance decreases when increasing μ variation. Therefore, the normalized error reaches its maximum value about 13% for a variation of -15%. Besides, it is clear that a variation of -15% affects results more seriously than a variation of $+15\%$. This is logic, since for a variation of -15%, μ becomes equal to 0.75 and the road surface is no more dry. However, for a variation of $+15\%$, μ reaches a value of 1.03, and we are always in the same dry road category.
   We believe that the observers, in their current configurations, could perform well on a dry and quasi-wet road, but it could not be the case for an iced road.

b) Comparing the EKF and UKF observers, it is shown that the O_{UKF} is less sensible to the road friction then the O_{EKF}.

To brief up, the integration of the lateral forces in the state vector using the relaxation-length concept, is a good way for an accurate estimation of these variables. However, we believe that taking into account significant μ variation in the estimation-process algorithm is fundamental for observers reliability.

2) Robustness With Respect to Parameters Variation: Vehicle parameters, such as mass, moments of inertia, and/or position of the COG, may vary significantly from one journey to the next. For example, when comparing a vehicle occupied only by the driver with a vehicle with passengers, additional luggage, and a full fuel tank, then the mass could easily vary by several hundred kilograms. In the next, we analyze the observers behavior with respect to the mass and yaw moment of inertia changes. To simplify the figures illustration, we focus on the rear tires behavior.

Loading conditions definitely affect the vehicle parameters and dynamic responses. In this study, the vehicle mass is assumed computed in the block 1 of the Fig. 1. The applied identification method approximates the vehicle's mass by monitoring the static suspension deflections at all the tire deflections [10], [11]. This method highly depends on the sensitivity of the used sensors, and may not lead precisely to the real vehicle mass. To study the robustness of O_{EKF} and O_{UKF} with respect to the vehicle mass m, we vary this parameter between -15% and $+15\%$ around the already used value. Fig. 21(a) and (b) shows that both observers are affected by the mass variations. Each bar in these figures correspond to a step variation of 5%. It is obvious that the normalized errors increase when increasing the mass variations. This is logical, since the system of equations (2), that describes the vehicle dynamics, introduces directly the vehicle mass. Moreover, errors in the load distribution induce significant errors in the vertical forces, which in turns affect considerably the lateral forces.

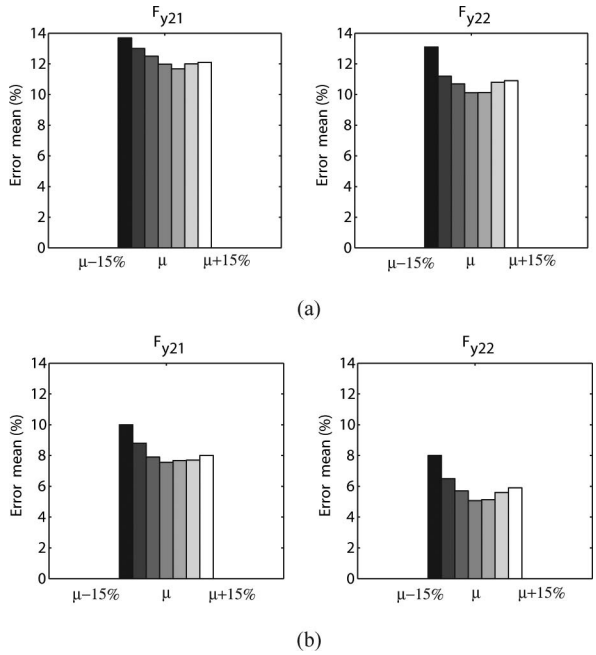

Fig. 20. Observers performance via road changes μ: -15%:5%:$+15\%$. (a) O_{EKF} robustness, μ varies between -15% and $+15\%$ around 0.9. (b) O_{UKF} robustness, μ varies between -15% and $+15\%$ around 0.9.

However, moment of inertia also varies with load conditions. Normally, I_z increases as the load increases. From Fig. 22(a) and (b), we can deduce that O_{UKF} and O_{EKF} are robust with respect to the yaw moment of inertia variations.

VII. Conclusion

This paper has presented a new method for estimating lateral tire forces and sideslip angle, that is, to say two of the most important parameters affecting vehicle stability and the risk of leaving the road. The two developed observers are derived from a simplified FWVM and are based on EKF and UKF techniques, respectively. Tire–road interaction is represented by a quasi-static Dugoff model.

A comparison with real-experimental data demonstrates the potential of the estimation process. It is shown that it may be

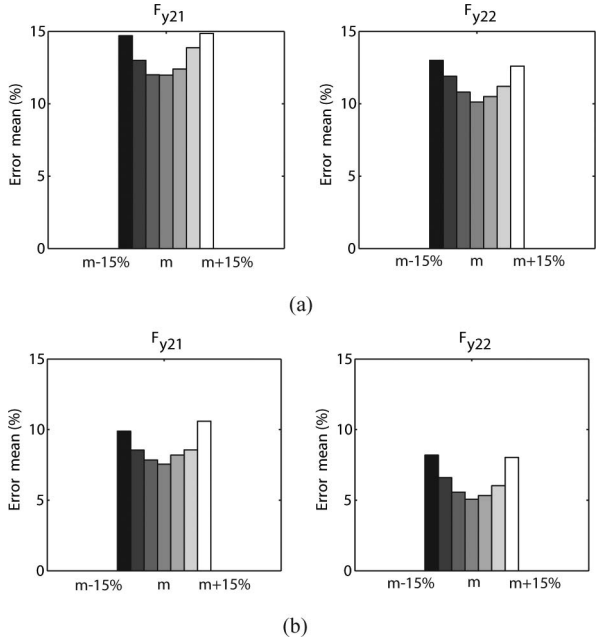

Fig. 21. Observers performance via mass changes m: -15%:5%:$+15\%$. (a) O_{EKF} robustness, m variation: -15% and $+15\%$ around 1550 kg. (b) O_{UKF} robustness, m variation: -15% and $+15\%$ around 1550 kg.

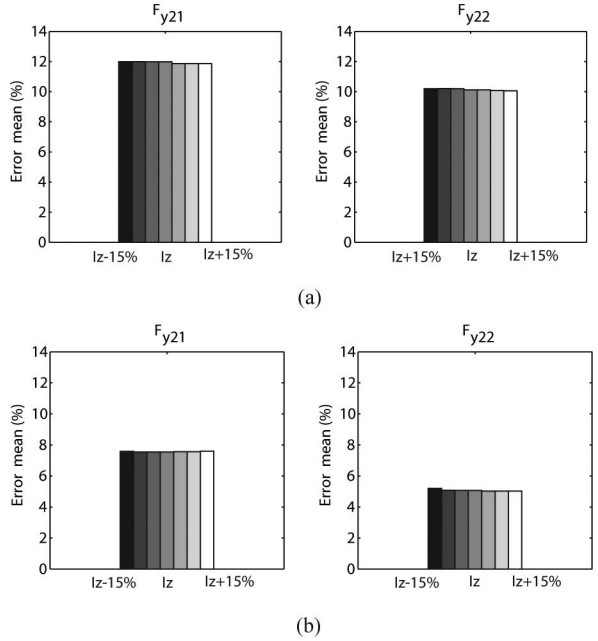

Fig. 22. Observers performance via I_z changes I_z: -15%:5%:$+15\%$. (a) O_{EKF} robustness, I_z variation: -15% and $+15\%$ around 2395 kgm^2. (b) O_{UKF} robustness, I_z variation: -15% and $+15\%$ around 2395 kgm^2.

possible to replace expensive correvit and dynamometric hub sensors by real-time software observers. This is one of the important results of our paper. Another important result concerns the estimation of individual lateral forces acting on each tire. This can be seen as an advance with respect to the current vehicle-dynamics literature.

Future studies will improve the vehicle/road model in order to widen validity domains for the observer, and make it adaptative with the road conditions (especially the road friction). Moreover, it will be of major importance to study the effect of coupling longitudinal/lateral dynamics on lateral tire behavior.

APPENDIX

In this Appendix, the principles of the EKF and UKF are summarized. A general stochastic state-space representation of nonlinear model has the form as follows:

$$\begin{cases} X_k = f(X_{k-1}, U_k) + w_k \\ Y_k = h(X_k) + v_k \end{cases} \tag{18}$$

where X and U are the state and input vectors, respectively, Y is the measurement vector, $f(.)$ and $h(.)$ are the states evolution function and the observation function, respectively, and w_k and v_k are the state disturbance and the observation noise vector, respectively. w_k and v_k are assumed to be gaussian, temporally uncorrelated and zero mean.

EKF algorithm

The fisrt-order EKF is presented as follows.

Initialization:

1) The initial state and the initial covariance are determined by

$$\bar{X}_0 = E[X_0], P_0 = E[(X_0 - \bar{X}_0)(X_0 - \bar{X}_0)^T].$$

Time Update:

2) The prediction of the state is given by

$$\bar{X}_{k|k-1} = f(\bar{X}_{k-1/k-1}, U_k)$$

3) The predicted covariance is computed as

$$P_{k|k-1} = AP_{k-1|k-1}A^T + Q$$

Measurement update:

4) The filter gain is calculated by

$$K_k = P_{k|k-1}H^T \left[HP_{k|k-1}H^T + R\right]^{-1}$$

5) The state estimation is determined by

$$\bar{X}_{k|k} = \bar{X}_{k|k-1} + K_k \left[Y_k - h(\bar{X}_{k|k-1}))\right]$$

6) The estimated covariance is

$$P_{k|k} = \left[I - K_k H\right] P_{k|k-1}$$

where A_k and H_k are the process and measurement Jacobians (matrix of all partial derivatives of a vector) at step k of the nonlinear equations around the estimated states, respectively,

$$A_k = \frac{\partial f(\overline{X}_{k-1/k-1}, U_k, 0)}{\partial X}$$

$$H_k = \frac{\partial h(\overline{X}_{k/k-1}, 0)}{\partial X}.$$

UKF algorithm

First, the state vector is augmented with the process and noise terms to give an $n^a = n + q$ dimensional vector

$$X_k^a = \begin{bmatrix} X_k & w_k \end{bmatrix}^T.$$

where $X \in R^n$ and $w \in R^q$. The process model is rewritten as a function of X_k^a

$$X_{k+1} = f\left[X_k^a, U_k\right].$$

According to [28], the UKF algorithm is presented as follows.

1) The set of $2n+1$ sigma points are created

$$\chi_{0,k|k} = \bar{X}_{k|k}$$

$$\chi_{i,k|k} = \bar{X}_{k|k} + \sqrt{(n+\lambda)P_{k|k}}, \quad i = 1, \ldots, n$$

$$\chi_{i,k|k} = \bar{X}_{k|k} - \sqrt{(n+\lambda)P_{k|k}}, \quad i = n+1, \ldots, 2n$$

and the associated weights

$$w_0^{(m)} = \kappa/(n+\kappa)$$

$$w_0^{(c)} = \kappa/(n+\kappa) + (1-\alpha^2+\beta_t)$$

$$w_i^{(m)} = 1/2(n+\kappa), i = 1, \ldots, 2n$$

$$w_i^{(c)} = 1/2(n+\kappa), i = 1, \ldots, 2n$$

where $\overline{X}_{k|k}$ and $P_{k|k}$ are the estimated state and covariance, respectively. α, β_t, and κ are related to the unscented transformation

$$\kappa = \alpha^2(n+\epsilon) - n.$$

As presented in Section V-D, α, β_t, and ϵ are set to 0.5, 2, and 0, respectively.

2) The transformed set is given by instantiating each point through the process model

$$\chi_{i,k+1|k} = f\left[\chi_{i,k|k}^a, U_k\right].$$

3) The predicted mean is computed as follows:

$$\overline{X}_{k+1|k} = \sum_{i=0}^{2n^a} w_i^{(m)} \chi_{i,k+1|k}^a.$$

4) The predicted covariance is computed as follows:

$$P_{k+1|k} = \sum_{i=0}^{2n^a} w_i^{(c)} \left\{\chi_{i,k+1|k} - \overline{X}_{k+1|k}\right\} \times \left\{\chi_{i,k+1|k} - \overline{X}_{k+1|k}\right\}^T.$$

5) Instantiate each of the prediction points trough the observation model

$$\gamma_{i,k+1|k} = h\left[\chi_{i,k+1|k}, U_k\right].$$

6) The predicted observation is calculated by

$$\overline{Y}_{k+1|k} = \sum_{i=0}^{2n} w_i^{(m)} \gamma_{i,k+1|k}.$$

7) Since the observation noise is additive and independent, the innovation covariance is as follows:

$$P_{(\xi\xi),k+1|k} = R + \sum_{i=0}^{2n^a} w_i^{(c)} \left\{\gamma_{k+1|k} - \overline{Y}_{k+1|k}\right\} \times \left\{\gamma_{k+1|k} - \overline{Y}_{k+1|k}^T\right\}^T.$$

8) The cross-correlation matrix is determined by

$$P_{(XY),k+1|k} = \sum_{i=0}^{2n^a} w_i^{(c)} \left\{\chi_{k+1|k} - \overline{X}_{k+1|k}\right\} \times \left\{\gamma_{k+1|k} - \overline{Y}_{k+1|k}^T\right\}^T.$$

9) Filter gain

$$K_{k+1} = P_{(XY),k+1|k} P_{(\xi\xi),k+1|k}^{-1}.$$

10) *Priori* covariance

$$P_{k+1|k+1} = P_{k+1|k} - K_{k+1} P_{(\xi\xi),k+1,k} K_{k+1}^T.$$

11) State estimation

$$\overline{X}_{k+1|k+1} = \overline{X}_{k+1|k} + K_{k+1}(Y_k - \overline{Y}_{k+1|k}).$$

Various extensions and modifications can be made to this basic method to take account of specific details of a given application. For example, if the observation noise is introduced in a nonlinear fashion, or is correlated with process and/or observation noise, then the augmented vector is expanded to include the observation terms.

REFERENCES

[1] F. Aparicio, J. Paez, F. Moreno, F. Jimenez, and A. Lopez, "Discussion of a new adaptive speed control system incorporating the geometric characteristics of the road," *Int. J. Veh. Auton. Syst.*, vol. 3, no. 1, pp. 47–64, 2005.

[2] Y. Hsu and J. Chistian Gerdes, "Experimental studies of using steering torque under various road conditions for sideslip and friction estimation," presented at the 2007 IFAC Symp. Adv. Autom. Control, Monterey, CA.

[3] D. Lechner, "Embedded laboratory for vehicle dynamic measurements," presented at the 9th Int. Symp. Adv. Veh. Control, Kobe, Japan, Oct. 2008.

[4] T. A. Wenzel, K. J. Burnham, M. V. Blundell, and R. A. Williams, "Estimation of the nonlinear suspension tyre cornering forces from experimental road test data," *Veh. Syst. Dyn.*, vol. 44, pp. 153–171, 2006.

[5] J. Dakhlallah, S. Glaser, S. Mammar, and Y. Sebsadji, "Tire-road forces estimation using extended Kalman filter and sideslip angle evaluation," presented at the Amer. Control Conf., Seatle, WA, Jun. 2008.

[6] L. R. Ray, "Nonlinear tire force estimation and road friction identification: Simulation and experiments," *Automatica*, vol. 33, no. 10, pp. 1819–1833, 1997.

[7] G. Baffet, A. Charara, and G. Dherbomez, "An observer of tire road forces and friction for active-security vehicle systems," *IEEE/ASME Trans. Mechatronics*, vol. 12, no. 6, pp. 651–661, Dec. 2007.

[8] G. Baffet A. Charara, D. Lechner, and D. Thomas, "Experimental evaluation of observers for tire-road forces, sideslip angle and wheel cornering stiffness," *Veh. Syst. Dyn.*, vol. 45, pp. 191–216, Jun. 2008.

[9] M. A. Wilkin, W. J. Manning, D. A. Crolla, and M. C. Levesley, "Use of an extended Kalman filter as a robust tyre force estimator," *Veh. Syst. Dyn.*, vol. 44, pp. 50–59, 2006.

[10] M. Doumiati, A. Victorino, A. Charara, and D. Lechner, "Lateral load transfer and normal forces estimation for vehicle safety: Experimental evaluation," *Veh. Syst. Dyn.*, vol. 47, no. 12, pp. 1511–1533, 2009.

[11] M. Doumiati, A. Victorino, A. Charara, D. Lechner, and G. Baffet, "An estimation process for vehicle wheel-ground contact normal forces," presented at the IFAC WC, Seoul Korea, Jul. 2008.

[12] U. Kiencke and L. Nielsen, *Automotive Control Systems*. Berlin, Germany: Springer-Verlag, 2000.

[13] Y. Hsu, "Estimation and control of lateral tire forces using steering torque," Ph.D. thesis, Stanford Univ., Stanford, CA, Mar. 2009.

[14] J. Dugoff, P. Fanches, and L. Segel, "An analysis of tire properties and their influence on vehicle dynamic performance," SAE Paper 700377, 1970.

[15] H. B. Pacejka, *Tyre and Vehicle Dynamics*. New York: Elsevier, 2002.
[16] T. D. Gillespie, *Fundamental of Vehicle Dynamics*. Warrendale, PA: SAE, 1992.
[17] R. Rajamani, *Vehicle Dynamics and Control*. Berlin, Germany: Springer-Verlag, 2005.
[18] S. L. Koo and H. S. Tan, "Tire dynamic deflection and its impact on vehicle longitudinal dynamics and control," *IEEE/ASME Trans. Mechatronics*, vol. 12, no. 6, pp. 623–631, Dec. 2007.
[19] H. Nijmeijer and A. J. Van der Schaft, *Nonlinear Dynamical Control Systems*. Berlin, Germany: Springer-Verlag, 1991.
[20] G. Baffet, "Développement et validation expérimentale d'observateurs des forces de contact pneumatique/chaussée d'une automobile," Ph.D. thesis, Univ. Technol. Compiègne, Compiègne, France, 2007.
[21] S. Drakunov and V. Utkin, "Sliding mode observers," in *Proc. IEEE Conf. Decis. Control*, 1995, pp. 3376–3379.
[22] J. Slotine, J. Hedrick, and E. Misawa, "On sliding observer for nonlinear systems," *J. Math. Syst. Estimation Control*, vol. 109, pp. 215–259, 1987.
[23] J. Slotine, J. Hedrick, and E. Misawa, "Computation of the observer gain for extended Luenberger observers using automatic differentiation," *IMA J. Math. Control Inf.*, vol. 21, pp. 33–47, 2004.
[24] R. E. Kalman, "A new approach to linear filtering and prediction problems," *Trans. ASME, J. Basic Eng. D*, vol. 82, pp. 35–45, 1960.
[25] G. Welch and G. Bishop, "An introduction to the Kalman Filter," Dept. Comput. Sci., Univ. North Carolina, Chapel Hill, NC, Tech. Rep. TR95-041, 1995.
[26] P. T. Venhovens and K. Naab, "Vehicle dynamics estimation using kalman filters," *Veh. Syst. Dyn.*, vol. 32, pp. 171–184, 1999.
[27] V. Sankaranayanan, M. E. Emekli, B. A. Gilvenc, L. Guvenc, E. S. Ozturk, E. S. Ersolmaz, and M. Sinal, "Semiactive suspension control of a light commercial vehicle," *IEEE/ASME Trans. Mechatronics*, vol. 13, no. 5, pp. 598–604, Oct. 2008.
[28] S. J. Julier and J. K. Uhlman, "A new extension of the Kalman filter to nonlinear systems," presented at the Int. Symp. Aerosp./Defense Sens., Simul. Controls, Orlando, FL, 1997.
[29] S. J. Julier, J. K. Uhlman, and H. F. Durrant-Whyte, "A new extension approach for filtering nonlinear systems," presented at the Int. Proc. Amer. Control Conf., Seattle, WA, 1995.
[30] M. R. Uchanski, "Road friction estimation for automobiles using digital signal processing methods," Ph.D. thesis, Univ. California, Berkley, CA, 2001.
[31] W. F. Milliken and D. L. Milliken, *Race Car Vehicle Dynamics*. Warrendale, PA: SAE, 1995.
[32] L. Haffner, M. Kozek, J. Shi, and H. Peter Jorgel, "Estimation of the maximum friction coefficient for a passenger vehicle using the instantaneous cornering stiffness," presented at the Amer. Control Conf., Seatle, WA, Jun. 2008.
[33] Y. Hsu and J. Chistian Gerdes, "Stabilization of a steer-by-wire vehicle at the limits of handling using feedback linearization," presented at the AMSE Int. Mech. Eng. Congress Expo. (IMECE 2005), Orlando, FL.

Moustapha Doumiati was born in Lebanon in 1983. He received the B.S. degree in electrical engineering from Lebanese University, Beirut, Lebanon, in 2005, and the M.S. degree in science of technology and information and the Ph.D. degree in automatic control from the Université de Technologie de Compiègne, Compiègne, France, in 2006 and 2009, respectively.

Since 2009, he has been a Postdoctoral Fellow at the Institut National Polytechnique de Grenoble, Grenoble, France. His current research interests include intelligent vehicles, driving assistance systems, state observers, linear parameter-varying systems, and robust control.

Alessandro Correa Victorino was born in Vitoria, Brazil, in 1973. He received the B.S. degree in mechanical engineering from the Federal University of Espirito Santo, Vitoria, Brazil, in 1996, the M.Sc. degree in mechanical engineering from the State University of Campinas, Campinas, Brazil, in 1998, and the Ph.D. degree for solving the self-localization and mapping problem, and autonomous navigation for mobile robots, embedded in a sensor-based navigation framework from the French National Institute of Automation and Computing Research, Nice, France, in 2002.

Since 2006, he has been an Associate Professor in the Computer Science Department, Université de Technologìe de Compiègne, Compiègne, France, where he has also been a Member of the Heudiasyc Laboratory, Centre National de la Recherche Scientifique. His current research interests include nonlinear state estimation, vehicle dynamics, cooperative perception systems, localization and mapping, sensor-based control, and navigation of autonomous systems.

Ali Charara (M'95) was born in Lebanon in 1963. He received the B.S. degree in electrical engineering from Lebanese University, Beirut, Lebanon, in 1987, the M.S. degree in automatic control from Energie et Traitement de l'information, Institut National Polytechnique de Grenoble, Grenoble, France, in 1988, and the Ph.D. degree in automatic control from the Universite de Savoie, Savoie, France, in 1992.

Since 1992, he has been an Assistant Professor in the Department of Information Processing Engineering, Université de Technologie de Compiègne, Compiègne, France, where he has also been the Director of the Heudiasyc Laboratory, Centre National de la Recherche Scientifique, since 2008 and became a Full Professor in 2003. His current research interests include intelligent vehicles, driving assistance systems, state observers, and diagnosis of electromechanical systems.

Daniel Lechner was born in France in 1959. He received the B.S. degree in fluid mechanics and the M.S. degree in mechanics from Energie et Traitement de l'information, Institut National Polytechnique de Grenoble, Grenoble, France, in 1981, and the Ph.D. degree in mechanics from the Ecole Centrale de Lyon, Ecully, France, in 2002.

In 1983, he joined the Department of Accident Mechanism Analysis (Salon de Provence), French National Institute for Transport and Safety Research, Bron, France, where he has been a Research Director since 2002, and is currently also an In-Charge. His research interests include vehicle modeling, instrumentation and testing, active safety embedded applications, and road accident analysis.